Dynamical critical behavior of isotropic ferromagnets

Christoph Hohenemser, Lee Chow,* and Robert M. Suter†
Department of Physics, Clark University, Worcester, Massachusetts 01610
(Received 10 May 1982; revised manuscript received 2 July 1982)

Experiments measuring the dynamical exponent z in the isotropic ferromagnets EuS, EuO, Ni, Fe, and Co are reviewed. Our recent hyperfine interaction experiments demonstrating crossover in z are described in detail. In contrast to early neutron experiments on isotropic ferromagnets it is found that with the exception of Co, pure Heisenberg behavior, i.e., $z=2.5$, is not observed in any of the materials surveyed. Instead, when either the wave number or the reduced temperature is sufficiently small, isotropic ferromagnets exhibit asymptotic behavior characterized by $z=2.0$. The most likely theoretical explanation is that significant spin-nonconserving forces are perturbing the Heisenberg exchange interaction. For ESR and neutron studies of EuS and EuO it has been shown that the observed behavior can be explained by dipolar forces. For hyperfine interaction experiments on Ni and Fe, the observed crossover to $z=2.0$ must be attributed to other, stronger spin-nonconserving forces. In the exceptional case of Co, where crossover to $z=2.0$ has not yet been observed, it is expected that future, more nearly asymptotic experiments, will detect crossover.

I. INTRODUCTION

At this time there is little doubt that static critical behavior of simple spin systems is well understood. Thus, for lattice dimension $d=3$ and spin dimension $n=1,3$, a detailed comparison of the best experiments with theory indicates agreement for the static critical exponent β to within $\sim 5\%$.[1]

In contrast, critical dynamics even for simple systems exhibit considerably greater complexity than static behavior. Thus, according to the recent review of Hohenberg and Halperin[2] for a given static university class (n,d), the dynamic exponent z depends on the equation of motion describing the order parameter, as well as the conservation laws that apply to the spin system. For example, the dynamic behavior for the isotropic antiferromagnet (e.g., $RbMnF_3$) is expected to be different than that for the isotropic ferromagnet (e.g., EuO). In the first case, the dynamic exponent is predicted to be $z=d/2=\frac{3}{2}$; in the second case, the prediction is $z=(d+2-\eta)/2\simeq\frac{5}{2}$.

Beyond this, recent work on high-T_c metallic ferromagnets Ni, Fe, and Co shows that there may be two dynamic critical regions in the same material, one characterized by the Heisenberg model, and one characteristic of order-parameter nonconserving systems.[3] Heisenberg behavior ($z\simeq\frac{5}{2}$) is observed in neutron scattering experiments at wave vectors $q\geq 0.05$ Å^{-1}; order-parameter nonconserving behavior ($z=2$) occurs in electron-spin-resonance (ESR) and hyperfine interaction experiments, both of which have significant contributions from the region near $q=0$.

The existence of two critical regions is most directly confirmed by experiments demonstrating crossover behavior. Above T_c, crossover has been observed in Fe and Ni by the present authors[4] via the technique of perturbed angular correlations; below T_c, crossover has been seen for Fe by Shaham *et al.*[5] via nuclear magnetic resonance (NMR).

Because our crossover experiments on Fe and Ni have been only briefly described,[4] the principal purpose of the present paper is to give a detailed account of this work, in an appropriate experimental and theoretical context. We begin with a statement of the theory and a review of the experiments which motivated our search for crossover in dynamical critical behavior.

II. THEORETICAL FRAMEWORK

For $T>T_c$, critical fluctuations are described by the correlation function for the ith spin component,[2]

$$S^{ii}(\vec{q},\omega)=2\pi[\omega_c^{ii}(\vec{q})]^{-1}S^{ii}(\vec{q})f_{\vec{q}}[\omega/\omega_c^{ii}(\vec{q})]\ . \tag{1}$$

Here $\omega_c^{ii}(\vec{q})$ is the linewidth of the fluctuations,

$S^{ii}(\vec{q})$ is the static or equal-time correlation function, $f_{\vec{q}}$ gives the energy line shape, and $\vec{q}$ and ω are the wave vector and energy of the fluctuations involved.

According to the static and dynamic scaling hypothesis[6] both $S^{ii}(\vec{q})$ and $\omega_c^{ii}(\vec{q})$ depend on the correlation length $\xi=1/\kappa$, which exhibits a power-law divergence at T_c, $\xi\sim t^{-\nu}$, where $t=|1-T/T_c|$. To express the scaling character of dynamic correlation function, $S^{ii}(\vec{q})$ and $\omega_c^{ii}(\vec{q})$ are each written as homogeneous functions of q and κ, having degree $-2+\eta$ and z, respectively,

$$S^{ii}(\vec{q})=q^{-2+\eta}g^{ii}(q/\kappa)\ , \tag{2}$$

$$\omega_c^{ii}(\vec{q})=q^z\Omega^{ii}(q/\kappa)\ . \tag{3}$$

Here η is the universal static exponent, z is the dynamic exponent on which our discussion is focused, and $g^{ii}(q/\kappa)$ and $\Omega^{ii}(q/\kappa)$ are nonsingular functions. The general forms of Eqs. (2) and (3) have been verified in a number of cases, including microscopic approximations, renormalization-group calculations,[2] and a range of neutron scattering experiments.[7]

By the definition of homogeneity[8] Eq. (3) implies

$$\omega_c^{ii}(\vec{q},\kappa)=\kappa^z\Omega_0^{ii}(\vec{q}/\kappa)\ , \tag{4}$$

where $\Omega_0^{ii}(\vec{q}/\kappa)=(\vec{q}/\kappa)^z\Omega^{ii}(\vec{q}/\kappa)$ is a nonsingular function. This means that $[\omega_c^{ii}(\vec{q})]^{-1}$, the lifetime of the fluctuations of wave vector $\vec{q}$, is dominated by a temperature dependence $t^{-z\nu}$, implying divergence as $T\to T_c$. Physically this is the well-known effect of "critical slowing down" which is common to all forms of critical dynamics. For a given static universality class ($\nu=$const), different values of z imply different temperature rates of critical slowing.

An alternative theoretical formulation of dynamic scaling is obtained on the assumption[9] that close to T_c for sufficiently large distances $\vec{r}$ (sufficiently small $\vec{q}$) the dynamic correlation function is a generalized homogeneous function. This means that for any λ, and exponents a and b,

$$S^{ii}(\lambda^a\vec{q},\lambda^b\omega)=\lambda S^{ii}(\vec{q},\omega)\ . \tag{5}$$

From this, by appropriate identification of a and b, it is straightforward to show that Eqs. (1)–(3) are recovered.

In whatever way dynamic scaling theory is formulated, it can give only *relations* between exponents, not exponent values themselves. Dynamic scaling is therefore a framework for describing fluctuations near T_c which incorporates some but not all the physics of the problem. However, the scal-

TABLE I. Exponent z for several model spin systems [adapted from P. C. Hohenberg and B. I. Halperin, Rev. Mod. Phys. 49, 435 (1977)].

Model spin system	Static universality class (n,d)	Possible examples	Conservation laws[a] Conserved	Conservation laws[a] Nonconserved	Scaling law for z	Approximate value of z for $d=3$
Heisenberg ferromagnet (model J)	$(3,d)$	EuO, EuS, $CrBr_3$, Fe, Ni, Co	ψ		$\frac{1}{2}(d+2-\eta)$	$\frac{5}{2}$
Heisenberg antiferromagnet (model G)	$(3,d)$	$RbMnF_3$	m	ψ	$d/2$	$\frac{3}{2}$
Anisotropic antiferromagnet (model C)	$(1,d)$	FeF_2, MnF_2	m	ψ	$2-\alpha/\nu$	2
Anisotropic ferromagnet (model C)	$(1,d)$	?	m	ψ	$2-\alpha/\nu$	2
Ferromagnets with significant relaxation due to phonons, dipolar interactions (model A)	(n,d)	High-T_c systems, e.g., Fe, Ni, Co. Dipolar systems, e.g., EuS, EuO		ψ	$2+c\eta$ $c=0.72(1-1.69)$	2

[a] ψ is the order parameter; m is an auxiliary conserved density such as the energy.

ing relations that connect the dynamic exponent z to static exponents can lead to quite accurate estimates of z if d, n, and relevant conservation laws are specified. This is because the combinations of static exponents that enter dynamic scaling relations for z are in the form of relatively small corrections (e.g., η and α/ν). To illustrate, we summarize in Table I the dynamical scaling results for five model spin systems, as discussed in the review by Hohenberg and Halperin.[2]

From Table I we see that dynamic scaling alone predicts that isotropic Heisenberg ferromagnets like Fe, Ni, Co, EuO, and EuS should exhibit a value of z close to $\frac{5}{2}$. The fact that some cases, as noted earlier, exhibit asymptotic values close to 2 must mean that either the anisotropy is sufficiently large (model C) or that order parameter nonconservation is sufficiently present (model A) to disturb pure Heisenberg behavior (model J). It was this basic insight that led us to suggest the existence of crossover between two critical regimes,[3] and that motivated our experimental research in Fe and Ni, as reported here.

III. PREVIOUS EXPERIMENTAL WORK ON ISOTROPIC FERROMAGNETS

To provide a context for our experiments, we begin with a review of previous experimental work on the critical dynamics of isotropic ferromagnets above T_c. We consider neutron scattering, electron-spin resonance, and hyperfine interactions in that order. The isotropic character of the systems studied allows suppression of spin components in the following. In effect we assume that the quantities of interest are independent of crystal orientation. This assumption is actually confirmed in the work of Shaham *et al.*[5] which we discuss in Sec. VIII.

A. Neutron scattering

The cross section for inelastic magnetic scattering of neutrons with momentum and energy transfer $\vec{q}$ and ω is

$$\sigma(\vec{q},\omega) \propto S(\vec{q},\omega) . \tag{6}$$

Thus neutron scattering, in principle, defines all aspects of spin motion near T_c. Experimentally the dynamic exponent z is found by measuring the energy linewidth of magnetic scattering as a function of $\vec{q}$ for $T=T_c$.[7] In this case Eq. (3) becomes

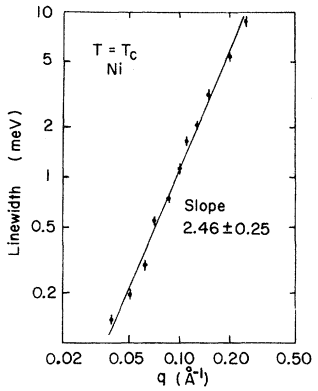

FIG. 1. Energy linewidth of magnetic neutron scattering as a function of q at $T=T_c$ for the case of Ni, as measured by Minkiewicz *et al.* (Ref. 10). The results indicate that $z=2.5$ for the range of q sampled.

$$\omega_c(\vec{q},\kappa)=q^z\Omega(\infty) , \tag{7}$$

and z may be determined directly from a log-log plot of ω_c vs q. To avoid the overwhelming effects of nuclear Bragg scattering near $q=0$ it is necessary in practice to restrict measurement to $q \geq 0.05$ Å^{-1}.

To illustrate the nature of neutron measurements, we show in Fig. 1 the results obtained by Minkiewicz *et al.*[10] for Ni. Results of neutron scattering experiments on isotropic ferromagnets are summarized in the top of Table II.[10–13] It is seen that apart from EuO, the measurements are consistent with $z=\frac{5}{2}$, as expected for Heisenberg ferromagnets with conserved order parameter (model J). For EuO, though the approach to $q=0$ is less close, the experimental value of z is substantially lower than $\frac{5}{2}$. A similarly low value $z=2.3$ (1) has been observed in Fe_3O_4, an isotropic ferrimagnet for which the order parameter is conserved and $z=\frac{5}{2}$ is theoretically expected.[14]

B. Electron-spin resonance

Zero-field ESR measures the electronic response function $\chi(\vec{q},\omega)$ directly. However, only the response at $q=0$ yields an appreciable signal. Heuristically speaking, for finite q, absorption in one part of the sample is canceled by emission in another. In terms of χ'', the imaginary or absorptive part of χ, the inverse linewidth evaluated at $q=0$ is

$$\omega_c^{-1}(0)=\lim_{\omega\to 0}[\chi''(0,\omega)/2\pi\omega\chi_s] . \tag{8}$$

In terms of χ', the real part of χ, the inverse linewidth is

TABLE II. Previous determination of z for Heisenberg ferromagnets.

Material	z	Range of q (Å^{-1})	Range of t	Ref.
Neutron scattering				
EuO	2.29(3)	0.12–0.48	at T_c	a
Ni	2.46(25)	0.04–0.2	at T_c	b
Fe	2.7(2)	0.05–0.2	at T_c	c
Co	2.4(2)	0.04–0.09	at T_c	d
ESR[e]				
EuO	2.04(7)	$q=0$	$3\times10^{-4}-10^{-1}$	f,g
EuS	1.88(6)	$q=0$	$10^{-3}-10^{-1}$	h
Hyperfine interactions[e]				
Ni	2.06(4)	all values	$10^{-4}-10^{-2}$	i,j
	2.07(34)	all values	$10^{-4}-2\times10^{-3}$	k
Fe	1.94(18)	all values	$10^{-4}-2\times10^{-3}$	l

[a]O. W. Dietrich, J. Als-Nielsen, and L. Passell, Phys. Rev. B 14, 4923 (1976).
[b]V. J. Minkiewicz, M. F. Collins, R. Nathans, and G. Shirane, Phys. Rev. 182, 624 (1969).
[c]V. J. Minkiewicz, Int. J. Magn. 1, 149 (1971).
[d]C. J. Glinka, V. J. Minkiewicz, and L. Passell, Phys. Rev. B 16, 4084 (1977).
[e]ESR and hyperfine interaction z values are obtained, respectively, from measurements of νz and $\nu(z-1-\eta)$, using theoretical values of ν and η.
[f]R. A. Dunlap and A. M. Gottlieb, Phys. Rev. B 22, 3422 (1980).
[g]J. Kötzler, W. Scheithe, R. Blickhan, and E. Kaldis, Solid State Commun. 26, 641 (1978).
[h]J. Kötzler, G. Kamleiter, and G. Weber, J. Phys. C 9, L361 (1976).
[i]R. C. Reno and C. Hohenemser, in *Proceedings of the Seventeenth Annual Conference on Magnetism and Magnetic Materials,* edited by D. C. Green and J. J. Rhyne (AIP, New York, 1972).
[j]A. M. Gottlieb and C. Hohenemser, Phys. Rev. Lett. 31, 1222 (1973).
[k]M. A. Kobeissi, R. M. Suter, A. M. Gottlieb, and C. Hohenemser, Phys. Rev. B 11, 2455 (1975).
[l]M. A. Kobeissi and C. Hohenemser, Hyperfine Interact. 4, 480 (1978). See also M. A. Kobeissi, Phys. Rev. B 24, 2380 (1981).

$$\omega_c^{-1}(0)=\chi_s/\Gamma\ , \tag{9}$$

where Γ is the $q=0$ Onsager kinetic coefficient defined by

$$\Gamma=\lim_{\omega\to0}\omega\{\chi_s/[\chi'^{-1}(0,\omega)-\chi_s^{-1}]\}^{1/2}\ . \tag{10}$$

Here χ_s is the static susceptibility. The exponent z may be deduced by measuring the reduced temperature dependence of $\omega^{-1}(0)$ or Γ. In the first case the susceptibility χ'' and χ_s must be determined, and Eq. (8) is used; in the second case the susceptibilities χ' and χ_s must be measured, and Eqs. (9) and (10) are used. From Eq. (4) it follows that

$$\omega_c^{-1}(0)=\text{const}\ t^{-\nu z}\ , \tag{11}$$

$$\Gamma=\text{const}\ t^{(\nu z-\gamma)}\ , \tag{12}$$

where γ is the static exponent describing the static susceptibility, i.e., $\chi_s\sim t^{-\gamma}$.

Working with EuO, Dunlap and Gottlieb[15] have measured χ'' and χ_s, and obtained $\omega_c^{-1}(0)$ vs t, as illustrated in Fig. 2 (top). For $t\lesssim10^{-2}$ a fit to Eq. (11) leads to the result $\nu z=1.42(5)$; with the use of $\nu=0.70$ (the Heisenberg value), $z=2.04(7)$ is obtained. Similarly, from a measurement of χ' and χ_s, Dunlap and Gottlieb[15] and Kötzler *et al.*[16] have obtained Γ vs t, as illustrated in Fig. 2 (bottom). $t\lesssim10^{-2}$ this indicates that $\Gamma\simeq$const, or via Eq. (12), that $z=\gamma/\nu=2$.

For $t\lesssim10^{-2}$ and $q=0$, EuO therefore shows asymptotic behavior that is characteristic of model A or C, not J. No vestige of pure Heisenberg behavior remains. Similar results have been obtained by Kötzler *et al.* for EuS (Ref. 17) and several other low-T_c nominally isotropic low-T_c ferromagnets.[18]

Available ESR and neutron scattering data on EuO thus give a reasonable and consistent picture of crossover in z from a noncritical region to an order-parameter nonconserving region. As we will

discuss in Sec. VIII, a consistent picture of these results may be obtained by invoking dipolar interactions.

What is not clear is whether the same behavior occurs in high-T_c ferromagnets like Ni, Fe, and Co, where ESR experiments are not available, and neutron results contain no hint of non-Heisenberg behavior. To approach this question we turn to our hyperfine interaction studies next.

C. Hyperfine interactions

Hyperfine interaction experiments involve observations of nuclear relaxation resulting from fluctuating electronic magnetic moments. The possible methods include NMR, perturbed angular correlations (PAC), and Mössbauer effect (ME). For isotropic, metallic ferromagnets we assume an interaction $\hbar A\vec{I}\cdot\vec{S}$ (nuclear spin I, electronic spin S). Under suitable restrictions (see below) this produces a nuclear relaxation rate τ_R^{-1}, directly proportional to the spin-autocorrelation time τ_c. For NMR the measured quantity is the spin–spin-relaxation rate T_2^{-1}, given by[19]

$$\tau_R^{-1}=T_2^{-1}=C_{\rm hf}^{\rm NMR}\tau_c=\tfrac{2}{3}S(S+1)A_g^2\tau_c \ . \quad (13)$$

For PAC one measures the time attenuation coefficient λ_2, of the perturbation factor $G_2(\tau)$ (see below), given by[20,21]

$$\tau_R^{-1}=\lambda_2=C_{\rm hf}^{\rm PAC}\tau_c=2S(S+1)A_e^2\tau_c \ . \quad (14)$$

For ME one determines the excess velocity linewidth $\Delta\Gamma_v$, of a γ ray of energy E, with the result that[22]

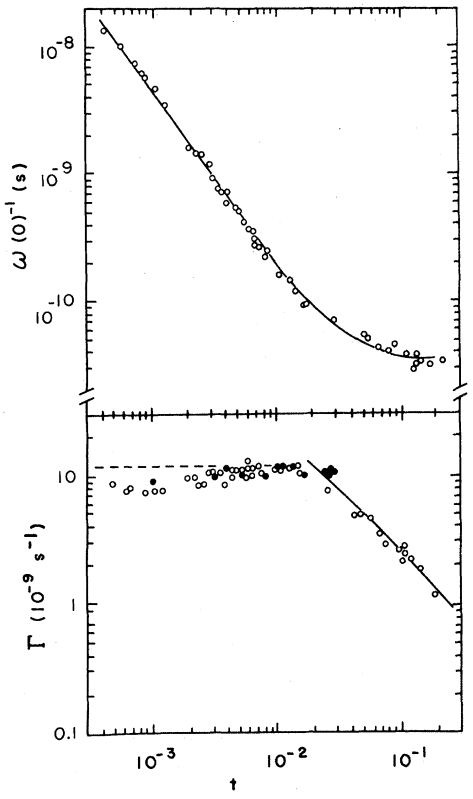

FIG. 2. Top: Temperature dependence of the inverse linewidth $\omega^{-1}(0)$ from zero-field ESR experiments on EuO. Bottom: Temperature dependence of the Onsager kinetic coefficient from zero-field ESR experiments on EuO. The open symbols in both cases are data of Dunlap and Gottlieb (Ref. 14); solid symbols in the bottom graph are Kötzler *et al.* (Ref. 15). Both sets of data yield $z\simeq 2$ for $t\leq 10^{-2}$.

$$\tau_R^{-1}=(E/\hbar c)\Delta\Gamma_v=C_{\rm hf}^{\rm ME}\tau_c \ , \quad (15a)$$

$$C_{\rm hf}^{\rm ME}=\tfrac{2}{3}S(S+1)\{A_e^2I_e(I_e+1)-A_eA_g[(I_e+I_g+1)^2/2-2]+A_g^2I_g(I_g+1)\} \ . \quad (15b)$$

The subscripts e and g refer to excited and ground nuclear states, respectively.

The isotropy of spin-relaxation times assumed in Eqs. (13)–(15) is directly demonstrated in NMR experiments on Ni, Fe, and Co,[5] as discussed in Sec. VIII. A restriction on Eqs. (13)–(15) is that τ_c must be the shortest time in the problem. For all three methods this means that $\tau_c\omega_L\ll 1$ and $\tau_c/\tau_R\ll 1$. In cases involving a finite nuclear lifetime τ_N, the additional experimental condition $\tau_c/\tau_N\ll 1$ applies. Together, these conditions are equivalent to the "motional narrowing" approximation in NMR, and have been shown to apply for all cases we shall discuss.

The spin-autocorrelation time τ_c is defined as the time average of the space-time–autocorrelation function $G(\vec{r},t)\,|_{r=0}$ as follows:

$$\tau_c\equiv\tfrac{1}{2}\int_{-\infty}^{\infty}dt[G(0,t)] \ . \quad (16)$$

Here $G(\vec{r},t)$ is the Fourier transform of $S(\vec{q},\omega)$ introduced in Eq. (1),

$$G(\vec{r},t)=V_q^{-1}\int_{V_q}\frac{\vec{d}q}{(2\pi)^3}\times\int_{-\infty}^{\infty}\frac{d\omega}{2\pi}e^{i(\vec{q}\cdot\vec{r}+\omega t)}S(\vec{q},\omega)\ , \tag{17}$$

and V_q is the volume of the Brillouin zone. Hence we have

$$\tau_c\propto\int_{V_q}\vec{d}q\,S(\vec{q},0)=\int_{V_q}\omega^{-1}(\vec{q})S(\vec{q})\vec{d}q\ . \tag{18}$$

The use of the dynamic scaling form for $S(\vec{q},0)$ implies

$$\tau_c\propto\int_{V_q}\vec{d}q\,q^{-2+\eta-z}\frac{f(\vec{q}/\kappa)g(\vec{q}/\kappa)}{\Omega(\vec{q}/\kappa)}\ . \tag{19}$$

For a spherical Brillouin zone of radius q_m this reduces to

$$\tau_c\propto\kappa^{d-2+\eta-z}\int_0^{q_m/\kappa}dx\,x^{d-3+\eta-z}\times\frac{f(x)g(x)}{\Omega(x)}\ . \tag{20}$$

In the critical region $q_m/\kappa\gg1$, and the upper limit in the integral may be replaced by ∞; from this it is clear that the integral is temperature independent, yielding

$$\tau_c\propto\kappa^{d-2+\eta-z}\propto t^{-w}\ , \tag{21}$$

where

$$w\equiv\nu(z+2-d-\eta)\ . \tag{22}$$

Thus measurements of τ_c vs t directly determine w, from which z is deducible by use of appropriate static exponents in Eq. (22).

The first hyperfine measurements of critical fluctuations in a ferromagnet were made on Ni by Reno and Hohenemser,[23] using the PAC technique on the (84−75)-keV $\gamma\gamma$ cascade of ^{100}Rh. These experiments were later repeated by Gottlieb and Hohenemser,[24] as illustrated in Fig. 3, and led to the results $w=0.70(3)$ and $z=2.06(4)$. Subsequently, ^{57}Fe Mössbauer spectroscopy work on Ni (Ref. 25) and Fe (Ref. 26) yielded equivalent, albeit less accurate results (see Table II). All available hyperfine data thus lead to z values in agreement with ESR work, but in disagreement with previous neutron data.

In contrast to neutron scattering and ESR, for which q is fixed at a given value and zero, respectively, hyperfine interactions involve a weighted sum of spin-relaxation times over all q, as expressed via Eq. (18). Depending on the weighting function $S(q)$, different regions of $\vec{q}$ space may be sampled. Thus, as $t\to0$, $S(q)$ becomes sharply peaked near $q=0$, and hyperfine experiments probe predominantly small q values. As t is increased the integrand is increasingly weighted by larger q, and hyperfine experiments may probe the same region of $\vec{q}$ space sampled by neutron scattering.

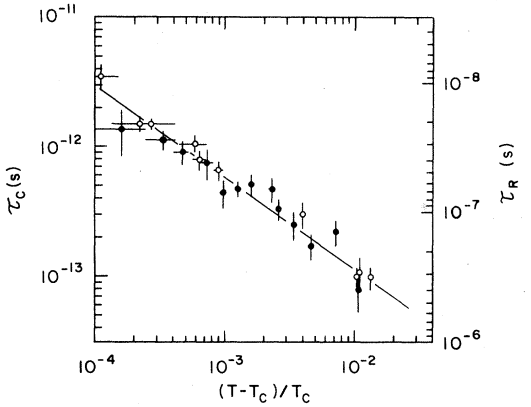

FIG. 3. Temperature dependence of the nuclear relaxation time τ_R from experiments in ^{100}Rh*Ni* by Reno and Hohenemser (open symbols, Ref. 23) and Gottlieb and Hohenemser (closed symbols, Ref. 24). Also shown is a scale for spin-autocorrelation time τ_c, calculated via Eq. (15a). The results indicate $z\simeq2$ over the temperature range sampled.

A reasonable explanation of the apparent contradiction between neutron and hyperfine results in Fe and Ni is therefore based on the fact that different regions of $\vec{q}$ space are sampled in each, and that these regions are dominated by different dynamical behavior. Based on this observation, Suter and Hohenemser[3] suggested in 1978 that the value $z=2$ seen in then existing hyperfine experiments may cross over to $z=2.5$ if sufficiently large values of reduced temperature are sampled. The crossover experiments described in this paper are therefore predicated on extending the temperature range over which τ_c is measured in hyperfine experiments.

IV. SELECTING A SYSTEM FOR TESTING CROSSOVER

In our past work we found that hyperfine experiments with radioactive probes are the most appropriate methods for extending the observation of critical dynamics in high-T_c metallic ferromagnets like Fe and Ni. Our principal reasons for this were

TABLE III. Sensitivity of various systems.

System	Nuclear properties[a] I (y)	γ (100 $G^{-1}s^{-1}$)	τ_N (ns)	Electronic properties[b] S	$H_{hf}(0)$ (kG)	Coupling constants A (10^9 s^{-1})	C_{hf} (10^{18} s^{-2})
		Perturbed angular correlation systems					
^{100}Rh*Fe*	2	102.4	310	1	−543	5.56	124.0
^{100}Rh*Ni*	2	102.4	310	$\frac{1}{2}$	−225	4.617	31.98
^{111}Cd*Fe*	$\frac{5}{2}$	−15.13	122	1	−348	0.525	1.10
^{111}Cd*Ni*	$\frac{5}{2}$	−15.13	122	$\frac{1}{2}$	−68	0.206	0.06
		Mössbauer spectroscopy systems					
^{57}Fe*Fe*	$I_e=\frac{3}{2}$	$\gamma_e=-4.95$	141	1	−337	$A_e=0.167$	0.387
	$I_e=\frac{1}{2}$	$\gamma_g=+8.66$				$A_g=-0.292$	
^{57}Fe*Ni*	$I_e=\frac{3}{2}$	$\gamma_e=-4.95$	141	$\frac{1}{2}$	−283	$A_e=+0.140$	0.409
	$I_g=\frac{1}{2}$	$\gamma_g=+8.66$				$A_g=-0.245$	
^{119}Sn*Fe*	$I_e=\frac{3}{2}$	$\gamma_e=+20.6$	25	1	−90	$A_e=-0.185$	1.54
	$I_g=\frac{1}{2}$	$\gamma_g=-100.3$				$A_g=+0.903$	
^{119}Sn*Ni*	$I_e=\frac{3}{2}$	$\gamma_e=+20.6$	25	$\frac{1}{2}$	+ 19	$A_e=+0.039$	0.103
	$I_g=\frac{1}{2}$	$\gamma_g=-100.3$				$A_g=-0.191$	
		Nuclear magnetic resonance systems					
^{61}Ni*Ni*	$\frac{3}{2}$	−23.95		$\frac{1}{2}$	−76	0.364	0.066
^{59}Co*Co*	$\frac{7}{2}$	+ 63.26		1	−226	1.36	2.46
^{57}Fe*Fe*	$\frac{1}{2}$	+ 8.66		1	−337	−2.92	0.114

[a]Nuclear properties include the spin I, the magnetogyric ratio γ, and the mean life τ_N.
[b]Electronic properties include the spin S and the hyperfine field $H_{hf}(0)$ at 0 K.

as follows.

(i) It is easy to do zero-field experiments above T_c. This is in contrast to NMR, for which zero-field relaxation is not measurable.

(ii) γ-ray detection from radioactivity-doped samples allows the use of very small samples, and requires no influx of energy as in the case of NMR and neutron scattering.

(iii) Radioactive impurity probes can be held to very low concentrations (~ 1 ppm) and do not involve serious problems with impurity-impurity interactions.

(iv) For appropriate nuclei, nuclear moments, lifetimes, and hyperfine fields are well matched to the range of nuclear relaxation times expected in the critical region.

Despite these advantages, the demands of crossover experiments are substantial. A principal problem is matching probe properties to the range of reduced temperature to be investigated. In going to larger and larger values of reduced temperature, as required by the crossover hypothesis, a given hyperfine coupling strength C_{hf} will produce increasingly longer nuclear relaxation times [see Eqs. (13)–(15)]. Eventually, when τ_R appreciably exceeds the nuclear lifetime τ_N, it will be impossible to measure τ_R with either the PAC technique or Mössbauer spectroscopy. Therefore, except for limitations imposed by time resolution in PAC and very broad lines in Mössbauer spectroscopy, the most favorable probe nucleus is one with the largest product $C_{hf}\tau_N$.

For isotropic ferromagnetic metals in a local-moment model of the hyperfine field the constant A (subscript e and g suppressed) may be approximated by

$$A=\gamma H_{hf}(0)/S\ , \tag{23}$$

where $H_{hf}(0)$ is the average hyperfine field at $T=0$ K and $\gamma=\mu_I/I\hbar$ is the magnetogyric ratio of the intermediate state. We have calculated coupling

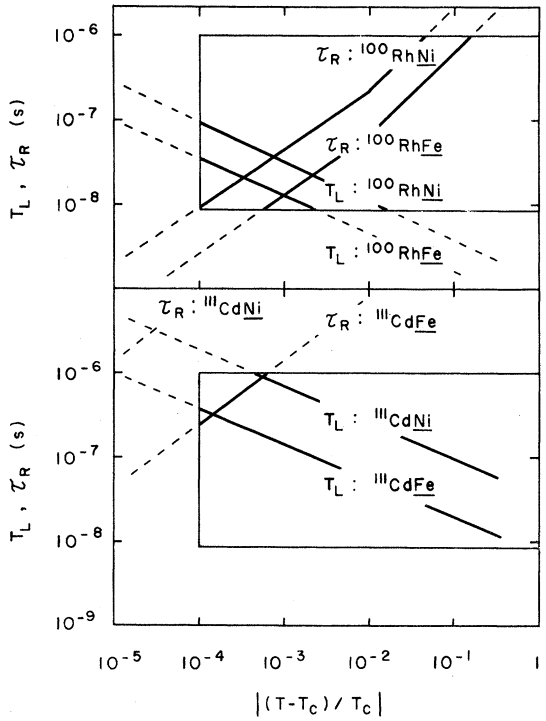

FIG. 4. Limits of reduced temperature constraining measurements of nuclear relaxation times τ_R via ^{111}Cd and ^{100}Rh PAC experiments. This shows that the ^{100}Rh probe is well matched to range of τ_R expected while ^{111}Cd is not.

constants C_{hf} [see Eqs. (13)–(15)], for several hyperfine probes and hosts, as shown in Table III. This indicates that the ^{100}Rh probe is the most sensitive, and most capable of detecting significant nuclear relaxation at large reduced temperature.

To estimate the expected range of accessible reduced temperature for various systems we have used the previous results on ^{57}Fe*Fe* and ^{100}Rh*Ni*, to make a plot of the expected behavior of τ_R vs t. We assumed $z=2.0$ for $t \leq 10^{-2}$ and $z=2.5$ for $t \geq 10^{-2}$ and drew a solid curve only over the region for which τ_R is detectable. For example, since the instrumental time resolution and nuclear lifetime for ^{100}Rh limit τ_R to $10 \leq \tau_R \leq 1000$ ns, the curves for ^{100}Rh*Fe* and ^{100}Rh*Ni* have been restricted to these values. We conclude from the results shown in Fig. 4 that the range of accessible reduced temperature is $6\times10^{-4} \leq t \leq 3\times10^{-1}$ and $10^{-4} \leq t \leq 6\times10^{-2}$ in Fe and Ni, respectively. Both should, therefore, allow detection of crossover near $t \geq 10^{-2}$. Also shown in Fig. 4 is the expected variation of the Larmor period T_L, below T_c. This indicates that for ^{100}Rh*Fe*, T_L falls below the instrumental time resolution already at $t=3\times10^{-4}$. Hence for ^{100}Rh*Fe*, unlike ^{100}Rh*Ni*, an independent determination of T_c from the temperature dependence of ω_L will not be possible because the nuclear precession will be "washed out."

The first experiments showing crossover in z near $t=10^{-2}$ above T_c were performed with ^{100}Rh*Fe* and ^{100}Rh*Ni* in 1979 at Clark University.[4] A full description of these experiments follows.

V. EXPERIMENTAL METHODS

A. Sample preparation

As in earlier work[23,24,27] 4-day ^{100}Pd was produced by ^{103}Rh $(p,4n)$ ^{100}Pd by bombarding 99.9%-pure natural Rh foil (100% ^{103}Rh) with 45-MeV protons at the Harvard cyclotron. After chemical separation of the Pd from the Rh target using a procedure developed by Evans,[28] Ni and Fe source foils were made by electroplating from 0.1 N $(NH_3)SO_4$ solution, followed by diffusion *in vacuo* at 1370 K for 4 h. Typical source foils had strengths of 3–5 μCi. Owing to stable Pd isotopes present as impurities in the Rh cyclotron target the total Pd concentration in our sources was estimated to be 300–600 ppm. Spectroscopic analysis per-

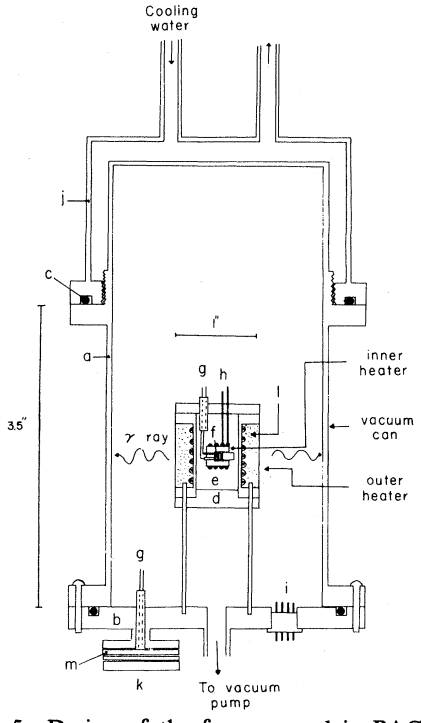

FIG. 5. Design of the furnace used in PAC experiments. *a*, aluminum vacuum can; *b*, brass bottom plate; *c*, rubber O ring; *d*; BN outer heater; *e*, BN inner heater; *f*, sample; *g*, thermocouple; *h*, heating element; *i*, heating element feedthrough; *j*, brass can; *k*, thermocouple feedthrough; *l*, fiberglass insulation; *m*, rubber insulation.

formed after each experiment yielded Pd concentrations in the range 100—1000 ppm, in agreement with our estimate.

B. Furnace design

To control the sample temperature near T_c we developed a furnace especially suited to PAC measurements. The furnace design, illustrated in Fig. 5 was adapted from an earlier Mössbauer oven designed by Kobeissi and Hohenemser.[29] As in the former, a double heater was used. To avoid excessive cooling requirements and to provide for a quicker response time of the feedback-controlled inner heater, the size of the controlled volume was reduced to less than 0.25 cm^3. In addition the new furnace provides greater freedom from corrosion, a considerably higher maximum temperature, good γ-ray transmission in all directions, and a long-term temperature instability of better than 0.05 K. During our experiments the furnace was operated for over 20 days without heater or thermocouple failure. The principal features of the furnace are summarized in Table IV and indicate that except in the area of γ-ray transmission, its specifications equal or exceed those of the earlier design in all respects. Details of the furnace's design and performance will be described elsewhere.

TABLE IV. Furnace characteristics.

Vacuum jacket	
Dimensions	Cylinder, 75-mm ϕ, 1.5-mm thick
Material	Aluminum
Cooling	Water, circulated continuously through 80-l reservoir to damp short-term fluctuations in temperature
Pressure	Less than 10^{-5} Torr; pumped by liquid-nitrogen trapped diffusion pump
Outer heater	
Dimensions	Cylinder, 25-mm ϕ, 25-mm high
Material	Machinable boron nitride
Heating element	8 Ω, iron-chromel 875 wire,[a] embedded in Aremco 503 paste[b]
Power level	60 W at 1100 K
Maximum temperature	1300 K.
Inner heater	
Dimensions	Cylinder, 6-mm ϕ, 6-mm high
Material	Machinable boron nitride
Heating element	1.5 Ω, iron-chromel 875 wire,[a] embedded in Aremco 503 paste[b]
Sample holder	Beryllium oxide disks, clamped with boron nitride plug
Thermocouples	
For 300—1000 K	0.25-mm ϕ chromel-alumel, having 0.04 μV/K at 1000 K
For 300—1400 K	0.13-mm ϕ W26&Re—W5&Re, having 0.018 μV/K at 1500 K
Dynamic characteristics	
Stability	0.03 K/h; 0.05 K/24 h
Response at 1000 K	10 s
γ-ray transmission	0.80 at 80 keV

[a]Manufactured by the Hoskins Manufacturing Co.
[b]Manufactured by Aremco Ceramics Inc.

C. PAC spectra

For measuring the temperature dependence of the nuclear relaxation time, as specified by Eq. (13), we utilized the (84—75)-keV $\gamma\gamma$ cascade of ^{100}Rh, as populated by 4-day ^{100}Pd. Detecting the first γ ray of the cascade with one counter, and demanding coincident detection of the second with another, ef-

fectively selects a population of nuclei with spin-polarized intermediate states. As a result, the emission probability of the second γ ray is anisotropic, and in the absence of extranuclear fields yields a time-independent correlation function,

$$W(\theta)=1+A_2P_2(\cos\theta)+\cdots , \tag{24}$$

where the ellipsis represents higher-order terms, and where θ is the angle between the cascade γ rays. For the (75–85)-keV cascade of ^{100}Rh used in the present work, the anisotropy coefficient is $A_2=0.173(4)$, and the higher-order terms are negligible.

In the presence of extranuclear perturbations the angular correlation function becomes dependent on the delay time τ between the γ rays. In this paper we are dealing with polycrystalline, nonmagnetized samples which near T_c have hyperfine field fluctuations leading to measurable nuclear relaxation, and below T_c have nonzero average values of the hyperfine field. In this case the correlation function is[21]

$$W(\theta,\tau)=1+A_2G_2(\tau)P_2(\cos\theta) , \tag{25}$$

with

$$G_2(\tau)=0.2\exp(-\tau/\tau_R)(1+2\cos\omega_L\tau+2\cos2\omega_L\tau) . \tag{26}$$

Here $\omega_L=\mu H_{\rm hf}/hI$ is the Larmor frequency of the intermediate-state moment μ in the time-averaged hyperfine field $H_{\rm hf}$, and τ_R is the nuclear relaxation time defined in Eq. (13).

In practice, the idealized form of $W(\theta,\tau)$ expressed in Eqs. (25) and (26) must be altered to reflect finite angular and time resolution. Angular averaging for cylindrical NaI(Tl) scintillation crystals has been treated by Yates[30] and leads to the replacement of $P_2(\cos\theta)$ by $\gamma_aP_2(\cos\theta)$, where $\gamma_a\leq1$ is an attenuation factor. Time averaging has been treated by Reno[31] among others, and for oscillatory perturbations leads to separate attenuation factors γ_1 and γ_2 for each frequency present. Assuming that τ_R is much larger than the experimental time resolution, we may write the angle- and time-averaged correlation function as

$$\overline{W}(\theta,\tau)=1+\gamma_a\overline{G}_2(\tau)P_2(\cos\theta) , \tag{27}$$

with

$$\overline{G}_2(\tau)=0.2\exp(-\tau/\tau_R)(1+2\gamma_1\cos\omega_L\tau+2\gamma_2\cos2\omega_L\tau) . \tag{28}$$

In our experiments we used a standard, four-counter scintillation spectrometer to record pairs of delayed coincidence spectra $C_{ij}(\theta,\tau)$ at angles $\theta=180°$ and 90°. Here the subscripts i and j refer to the individual counters involved ($i,j=1,2,3,4$). The measured coincidence spectra are then related to the correlation function via

$$C_{ij}(\theta,\tau)=C_0\exp(-\tau/\tau_N)\overline{W}(\theta,\tau)+B_{ij} , \tag{29}$$

where τ_N and B_{ij} are the intermediate-state lifetime and the accidental background, respectively.

D. PAC data reduction

To arrive at the desired physical quantities it is necessary to eliminate irrelevant variables such as τ_N, B_{ij}, and C_0 as well as single-counter and coincidence efficiencies. Especially for long relaxation times τ_R, this is not a trivial problem. As indicated recently by Arends *et al.*[32] a general approach is to form appropriate counting-rate ratios. Under favorable conditions these reduce to functions of $\overline{W}(\theta,t)$ alone.

For the case of ^{100}Rh*Fe* four counters were used to produce two pairs of coincidence spectra for counter angles $\theta=180°$ and 90°, respectively. The spectra for each angle were electronically added, stored in two halves of an analyzer memory, and reduced via

$$R(\tau)=\frac{2[C^+(180,\tau)-C^+(90,\tau)}{C^+(180,\tau)+2C^+(90,\tau)} , \tag{30}$$

where C^+ refers to background-subtracted, summed spectra normalized to the same number of total counts. Assuming that the background subtraction is reliable, and that coincident efficiencies cancel, this implies[32]

$$R(\tau)=\frac{2[\overline{W}(180,\tau)-\overline{W}(90,\tau)}{\overline{W}(180,\tau)+2\overline{W}(90,\tau)} . \tag{31}$$

For the case of ^{100}Rh*Ni*, where large values of τ_R require a more reliable treatment of the accidental background, all four coincidence spectra were stored separately, and *without* prior background subtraction, reduced via

$$R(\tau)=\frac{2[C_{13}(180,\tau)-\alpha C_{23}(90,\tau)]}{C_{13}(180,\tau)+2\alpha C_{23}(90,\tau)} , \tag{32}$$

with

$$\alpha \equiv \left[\frac{C_{13}(180,\tau)C_{14}(90,\tau)}{C_{23}(90,\tau)C_{24}(180,\tau)} \right]^{1/2} . \quad (33)$$

If, as before, cancellation of coincidence efficiencies is assumed, this form of $R(\tau)$ also leads to Eq. (31).

Because we cannot be sure that coincidence efficiencies cancel in either of the above reduction schemes, we expect that Eq. (31) is modified by an additive constant R_0, consisting of products of coincidence efficiencies.[32] Combining Eqs. (27), (28), and (31) then leads to the general form

$$R(\tau)=R_0+0.2A_2\gamma_2\exp(-t/\tau_R) \times(1+2\gamma_1\cos\omega_L\tau+2\gamma_2\cos2\omega_L t) . \quad (34)$$

Equation (34) was used in fitting all of our data. In these fits R_0, $\gamma_a A_2$, τ_R, γ_1, γ_2, and ω_L were treated as free parameters.

VI. RESULTS ON ^{100}Rh*Fe*: $T > T_c$

Typical nuclear relaxation spectra for ^{100}Rh*Fe* above T_c are shown in Fig. 6. Fitted values of τ_R obtained for $1043.6 \leq T \leq 1198.15$ are listed in Table V. These were converted to spin-autocorrelation times via Eq. (14) and $C_{\rm hf}$ as given in Table III. The value of T_c was obtained from the observed behavior of $R(\tau)$, as predicted by Eq. (34). Well below T_c, because ω_L^{-1} becomes less than the instrumental time resolution, $\gamma_1=\gamma_2=0$, and we expect

$$R(\tau)=0.2A_2\gamma_a\exp(-\tau/\tau_R)+R_0 . \quad (35)$$

In contrast, well above T_c, with $\omega_L=0$, $\gamma_1=\gamma_2=1$,

$$R(\tau)=A_2\gamma_a\exp(-\tau/\tau_R)+R_0 . \quad (36)$$

For the time-dependent portion of $R(\tau)$ we therefore expect a smooth transition from an amplitude of $0.2A_2\gamma_a$ far below T_c to an amplitude $A_2\gamma_a$ *just above* T_c. In principle, T_c may therefore be defined as the temperature where the time-dependent part of $R(\tau)$ just reaches maximum amplitude as T_c is approached from below. In practice there is some rounding in the transition because of the effect of time resolution in the region of very short nuclear relaxation just above T_c.

By fitting the data near T_c to

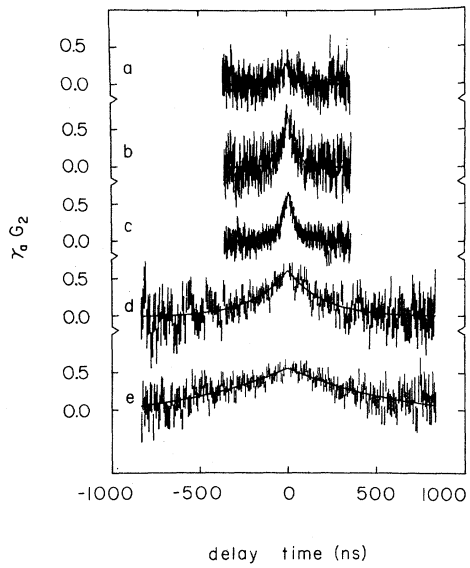

FIG. 6. Typical anisotropy relaxation spectra obtained in experiments on ^{100}Rh*Fe*. The temperatures, from top to bottom, are as follows: 1028.15, 1045.15, 1054.15, 1094.15, and 1148.15 K, respectively. The value T_c is 1042(2) K. The top spectrum is therefore well below T_c, and exhibits only the hard-core anisotropy for reasons explained in the text.

$$R(\tau)=a\exp(-\tau/\tau_R)+b , \quad (37)$$

with a, b, and τ_R free, the points shown in Fig. 7 were obtained. This indicates that $R(\tau)$ behaves as

TABLE V. τ_R and τ_c values for ^{100}Rh*Fe*.

$(T-T_c)/T_c$[a] (10^{-4})	τ_R (ns)	τ_c (10^{-14} s)
15.8	25(4)	32(5)
25.4	26(4)	31(5)
30.2	29(5)	28(5)
35.0	23(3)	35(5)
37.4	30(6)	27(5)
39.8	33(5)	24(4)
49.4	35(4)	23(3)
68.6	39(4)	21(3)
116.6	53(5)	15(1)
222.2	99(14)	8.1(1.2)
308.5	126(14)	6.4(7)
303.4	151(18)	5.3(6)
500.5	216(39)	3.7(7)
606.0	269(45)	3.0(5)
702	300(59)	2.7(5)
855	381(110)	2.1(6)
1018	449(26)	1.8(1)
1498	960(180)	0.8(2)

[a]Error in reduced temperature is 2×10^{-3}.

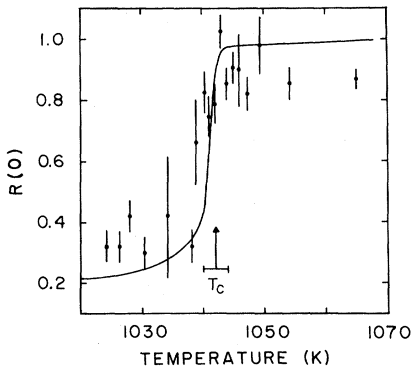

FIG. 7. Determination of T_c from the zero-time anisotropy $R(0)$ as described in the text.

expected. The actual value of T_c was determined by comparing the shape of the experimental data to the shape of a computer simulation (Fig. 7, solid curve). For the latter, $\omega_L(t)$ and $\tau_R(t)$ were estimated from the results of previous Mössbauer experiments[26] and the experimental time-resolution curve was explicitly folded in. With the use of the resulting estimate of $T_c=1042(2)$ K, absolute temperatures were converted to reduced temperatures, as shown in Table V.

A plot of τ_R and τ_c against t is shown in Fig. 8 (closed symbols). A fit to the region $t \leq 10^{-2}$ with

$$\tau_R = Dt^w , \tag{38}$$

yields $D=2.3(2)\times 10^{-15}$ s and $w=1.08(5)$. With the use of the scaling law of Eq. (22) and theoretical values $\nu=0.70$ and $\eta=0.034$ obtained by LeGuillou

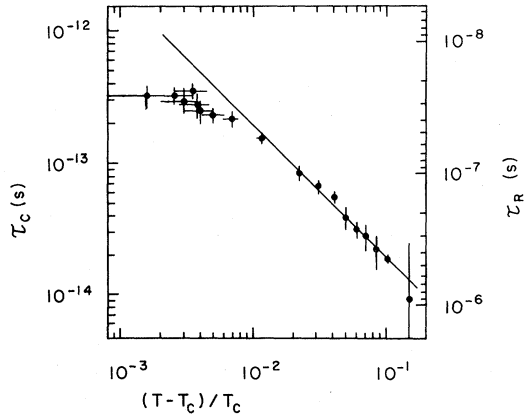

FIG. 8. Temperature dependence of the nuclear relaxation time τ_R, from experiments on ^{100}Rh*Fe*. Also shown is a scale for the spin-autocorrelation time τ_c calculated via Eq. (15a). The data for $t \geq 10^{-2}$ indicate $z \simeq 2.5$, with crossover toward a lower value near $t=10^{-2}$.

et al. via the renormalization group,[33] this implies $z=2.60(8)$. Because of the large error in T_c, the region $t \leq 10^{-2}$ could not be reliably fitted.

The experiments on ^{100}Rh*Fe* therefore demonstrate clearcut $d=3$ Heisenberg dynamical behavior for $t \geq 10^{-2}$, consistent with neutron scattering. For $t \leq 10^{-2}$ they show a tendency toward weaker singular behavior, consistent with earlier Mössbauer work[26] that lead to $z \simeq 2$ for $t \leq 2\times 10^{-3}$. Together these observations represent strong confirmation of our crossover hypothesis in the case of Fe.

VII. RESULTS ON ^{100}Rh*Ni* FOR $T > T_c$

Previous ^{100}Rh PAC experiments on critical fluctuations in Ni led to the conclusion that $z=2.0$ for $t \leq 10^{-2}$.[23,24] The purpose of the present work was therefore to extend the temperature region sampled.

Typical nuclear relaxation spectra are shown in Fig. 9. Fitted numerical values of τ_R obtained for $627.65 \leq T \leq 664.25$ K are given in Table VI, bottom. Previous results obtained, respectively, by Gottlieb and Hohenemser[24] and Reno and Hohenemser[23] are given in Table VI, middle and top.

The τ_R values were converted to τ_c values via Eq. (14) and the value of $C_{\rm hf}$ given in Table III. The value of T_c was obtained separately for each of the

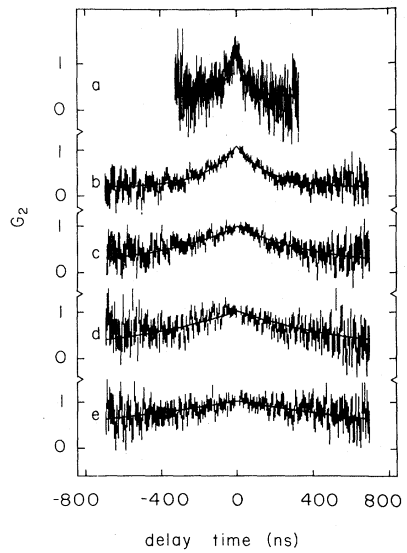

FIG. 9. Typical anisotropy relaxation spectra obtained in experiments on ^{100}Rh*Ni*. The temperatures from top to bottom are 628.15, 633.15, 639.15, 645.15, and 662.25 K. The value of T_c determined from Larmor precession measurements below T_c is $T_c \simeq 627.5(3)$ K.

TABLE VI. τ_R and τ_c values for ^{100}Rh*Ni*.

$(T-T_c)/T_c$ (10^{-4})	τ_R (ns)	τ_c (10^{-14} s)
Data of Reno and Hohenemser		
1.58	23(9)	136(35)
3.33	28(5)	112(17)
4.76	34(7)	92(16)
7.30	42(11)	74(15)
9.68	71(17)	44(8)
12.7	67(10)	47(7)
16.0	62(13)	51(9)
20.3	67(14)	47(8)
26.3	96(18)	33(7)
34.4	127(32)	25(5)
46.5	189(47)	17(6)
71.7	143(34)	22(4)
108	401(132)	7.8(19)
Data of Gottlieb and Hohenemser		
1.11	9(2)	348(63)
2.23	21(3)	149(18)
2.70[a]	21(2)	149(12)
5.90[a]	30(5)	104(10)
6.48	40(7)	78(11)
9.00	48(8)	65(9)
40.0	105(25)	30(6)
105	320(67)	9.8(17)
110	292(88)	10.7(18)
134	322(67)	9.7(17)
This work		
2.4[a]	36(9)	87(17)
6.4[a]	45(6)	70(9)
10.3	58(7)	54(6)
13.5	65(8)	48(5)
34	124(8)	25(2)
60	189(10)	16.6(9)
90	185(7)	16.9(7)
185	430(20)	7.3(3)
281	650(60)	4.8(4)
378	1030(130)	3.0(3)
586	1490(150)	2.1(2)

[a]Error in $(T-T_c)/T_c$ is 1.5×10^{-4}. All other points have an error of 0.9×10^{-4}.

three sets of data by fitting measurements of $\omega_L(T)$ below T_c with

$$\omega_L(T)=B(1-T/T_c)^{\beta}, \tag{39}$$

where B and T_c are treated as free, and the exponent β was fixed at 0.385, as found by Reno and Hohenemser.[34] Given values of T_c, reduced temperatures were calculated for each set of data, as shown in Table VI.

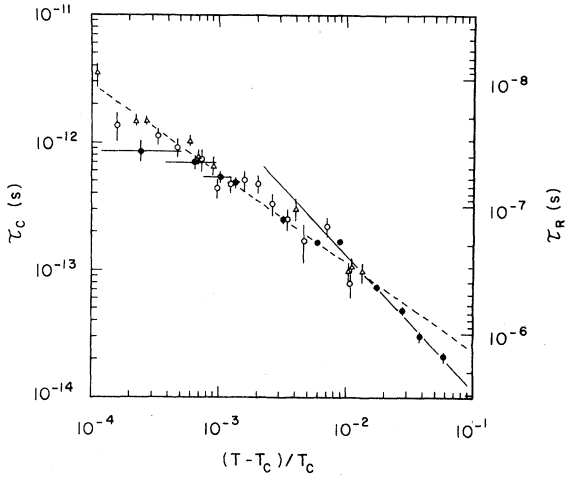

FIG. 10. Temperature dependence of nuclear relaxation time τ_R from experiments on ^{100}RhNi. The plot combines the previous data (open symbols, Refs. 23 and 24) and the results of the present experiments (closed symbols). Also shown is a scale for the spin-autocorrelation time τ_c calculated via Eq. (15a). The results indicate crossover from $z\simeq2.5$ to $z=2.0$ near $t\simeq10^{-2}$.

A plot of τ_R and τ_c vs t is shown in Fig. 10. This includes both new results and those obtained previously. For $5\times10^{-4}\leq t\leq10^{-2}$ the new data agree well with the previous results. For $10^{-2}\leq t\leq6\times10^{-2}$ τ_c decreases more rapidly, suggesting crossover. As shown in previous work, a fit to $\tau_c=Dt^{-w}$ with D and w free yields $w=0.70(3)$, $D=4.7(4)\times10^{15}$ s, and $z=2.06(4)$ for $t\leq10^{-2}$. For $t\geq10^{-2}$ in contrast, we obtain $w=1.0(2)$, $D=1.1(2)\times10^{-15}$ s, and $z=2.5(2)$.

The study of ^{100}Rh*Ni*, like ^{100}Rh*Fe*, thus demonstrates $d=3$ Heisenberg dynamical behavior for $t\geq10^{-2}$, i.e., $z=2.5$. For $t\leq10^{-2}$ there is clearcut crossover to a lower value of z, which in contrast to the case of Fe, can be determined to an accuracy of 5%.

VIII. A COMPARISON TO NMR EXPERIMENTS BELOW T_c

It is interesting to compare our results on Ni and Fe to recent NMR data obtained by Shaham, Barak, El-Hanany, and Warren.[5] Through a combination of well-thoughtout precautions (bulk instead of powder samples to reduce thermal gradients, isotopic enrichment, and toroidal sample

geometry to improve fill factors) these authors were able to perform the first NMR investigations of the critical region of Ni, Co, and Fe. Though their study includes Knight-shift data above T_c, their critical dynamics data below T_c are of the greatest interest for our present purpose.

Their results may be summarized as follows:

(1) For all three metals, the longitudinal relaxation time T_1 approaches the transverse relaxation time T_2 as the temperature approaches T_c from below, i.e., $T_1 = T_2$ in the critical region.

(2) For each metal, the relaxation rate T_1^{-1} and/or T_2^{-1} shows a strong divergence as T_c is approached from below.

(3) The power law describing this divergence yields dynamic exponent values of $z'=2.0$ for Ni, $z'=2.5$ for Co, and shows crossover from $z' \geq 2.5$ to $z'=2.0$ for Fe.

The first finding serves as an explicit confirmation of our earlier assumption (Sec. III) that near T_c, spin fluctuations are isotropic. The second finding indicates that, as expected, critical slowing occurs below as well as above T_c. The third finding suggests that a quantitative comparison of the NMR data and our PAC and ME data might be profitable.

We have therefore used the coupling constants in Table III and measured τ_R values to calculate τ_c values in a consistent manner for all available hyperfine data in Ni, Co, and Fe. The results, illustrated in Fig. 11, indicate that within a factor of ± 2 different experiments yield the same τ_c values at comparable reduced temperature, and that within the same factor, τ_c values are symmetrical about T_c.

Beyond this remarkable simplicity, there are some distinct differences in behavior. (1) Crossover

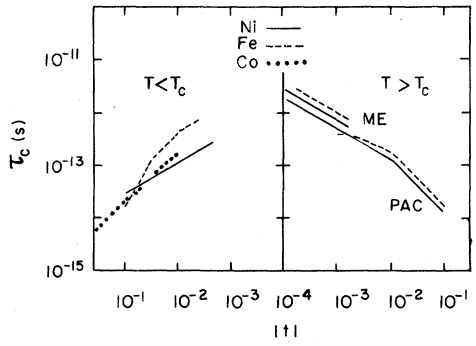

FIG. 11. Comparison of spin-autocorrelation times τ_c calculated from NMR data below T_c (Ref. 5) and PAC and ME data above T_c (Refs. 4, 23–26, and this work).

for Ni, seen above T_c, is not repeated below T_c, and crossover in Fe, seen below T_c, is only roughly indicated in the data above T_c. (2) For the same host, differences in τ_c appear to be systematically related to the utilization of different hyperfine probes. Both effects may reflect experimental limitations, and not intrinsic properties of critical dynamics. Thus, the apparent lack of exact crossover symmetry is probably due to the fact that, with the exception of the ^{100}RhNi data, individual experiments cover less than two decades in reduced temperature. The apparent differences in τ_c for the same host could also result from the fact that the hyperfine Hamiltonian used and the spin assignments made in Table III are at best an approximation to the more complex behavior of metallic magnetic systems.

IX. THE CAUSES OF CROSSOVER

According to our theoretical picture crossover in z results from competition between the short-range Heisenberg interaction, which conserves spin, and one or more long-range, spin-nonconserving interactions. Our review of experimental results has shown that pure Heisenberg behavior occurs in no case in which sufficiently small values of q are sampled.

Interestingly, evidence for competition between different interactions is not limited to critical phenomena. In spin-wave theory[35] an unmodified Heisenberg exchange interaction leads to small-q spin-wave dispersion with energy $E \propto q^2$; in contrast, addition of noncommuting terms to the Hamiltonian implies for small q that $E \propto q$. Experimentally, corresponding crossover in q has been seen in neutron scattering experiments on Fe,[10] according to which $E = 281q^2 - 275q^4$ for $0.2 \leq q \leq 0.6$ Å^{-1} and $E \sim q$ for $0.02 \leq q \leq 0.05$ Å^{-1}.

One question remains: What are the causes of crossover in dynamics? Hohenberg and Halperin[2] argue $z=2.0$ could be produced either by sufficiently large anisotropy in the short-range exchange interaction (model C) or the presence of long-range spin-nonconserving perturbations (model A).

A. Spin-nonconserving forces

To explain crossover in z requires perturbations that are dominant at long range, i.e., small q, and that do not conserve total spin. Dipolar interactions, pseudodipolar interactions, spin-lattice forces, and itinerant electron interactions appear to be four

plausible candidates. Of the four, itinerant electron interactions can probably be eliminated since it has been shown by Hertz[36] that $z=\frac{5}{2}$ in this case.

True dipolar interactions arise from the interaction between freely orientable spins such as found in S-state systems like EuO and EuS. Crossover for this case has been studied by Huber,[37] Maleev,[38] Teitelbaum,[39] and Raghavan and Huber.[40] Consistent with model A of Hohenberg and Halperin, all but Maleev predict that $z=2$ for small q. For $q=0$ Huber[37] has obtained a crossover-reduced temperature t_d, which is, in effect, the ratio of the dipolar to the exchange interaction strength,

$$t_d=\frac{g^2\mu_B^2/a^3}{S(S+1)k_BT_c} . \tag{40}$$

Here $g\mu_B$ is the electronic dipole moment, a the nearest-neighbor distance, and k_B Boltzmann's constant.

Pseudodipolar interactions arise from the interplay of spin dipoles with orbital angular momentum, and were originally postulated by van Vleck[41,42] to explain the experimentally observed anisotropy in Fe and Ni. According to van Vleck's 1937 paper, pseudodipolar forces for Fe and Ni are about 50 times stronger than true dipolar coupling. This has been confirmed more recently by Joenk,[43] who has used measured anisotropy constants for Fe, Ni, and fcc Co to conclude that the ratio of pseudodipolar to true dipolar coupling is 93, 140, and 98, respectively. Since the pseudodipolar and true dipolar interactions have the same mathematical form, it seems reasonable to use Eq. (40) with an appropriately increased coupling constant for estimating the crossover-reduced temperature.

Unlike dipolar interactions, the spin-lattice interaction has received little attention as a cause of crossover. It is an attractive candidate because it does not commute with the total spin, and increases linearly with temperature. If the crossover temperature t_{sl} is proportional to the ratio of the perturbation to the exchange strength as in Eq. (39), one should expect that t_{sl} is approximately independent of T_c.

B. Application to specific materials

1. EuO and EuS

Since these are S-state systems it is natural to consider true dipolar interactions as the most likely explanation of the observed results. As shown in the literature, this approach works well.

Thus Dunlap and Gottlieb[15] have noted that the boundary of the $z=2.0$ region for EuO corresponds well with the estimate of $t_d\simeq 5\times 10^{-2}$ provided by Eq. (40). Comparable conclusions may be drawn from the ESR work of Kötzler and collaborators on EuO,[16] EuS,[17] and other, nominally isotropic low-T_c ferromagnets.[18]

Similarly, Dietrich *et al.*,[13] in measurement of the neutron scattering linewidth in EuO at $T=T_c$, have explained the anomalous result, $z=2.29(3)$, by the fact that the range of q sampled just spans $q_d=0.16$ Å^{-1}, the estimated dipolar crossover wave vector.

Gottlieb and Dunlap[15] further point out that crossover in q observed at $T=T_c$ in neutron scattering is quantitatively consistent with crossover in t observed at $q=0$ via ESR. In effect, they argue that crossover at t_d defines a particular value of the inverse correlation length, $\kappa_d=\kappa_0 t_d^{\nu}$, where in general $\kappa=\kappa_0 t^{\nu}$. Given the homogeneous nature of the linewidth function [Eqs. (3) and (4)] and the equivalent roles of q and κ, it is reasonable to assume that the dipolar crossover wave vector is

$$q_d=\kappa_d=\kappa_0 t_d^{\nu} . \tag{41}$$

Using this relation and a value of t_d obtained from Eq. (40), it is found that $q_d=0.16$ Å^{-1}, consistent with the predicated crossover character of the neutron data. The regions of (q,κ) space for EuO sampled by ESR and neutron scattering are illustrated in Fig. 12.

2. Fe and Ni

Consider that hyperfine experiments determine $t_x(\bar{q})$, a crossover temperature involving an average over all q. It may be shown that $t_x(\bar{q})$ is a good estimate of, though somewhat less than $t_x(0)$, the

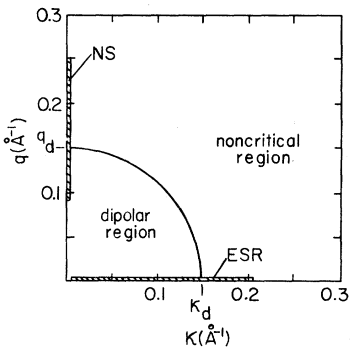

FIG. 12. Estimated dipolar and noncritical region for EuO, with indication of locus for neutron scattering data (NS) and ESR data along the vertical and horizontal axes, respectively.

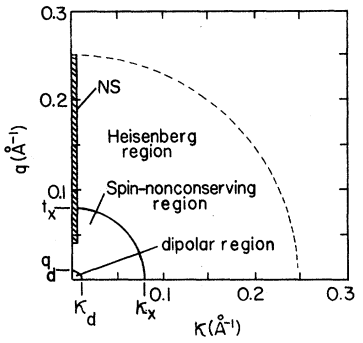

FIG. 13. Estimated dipolar, spin-nonconserving, and Heisenberg region for Fe, with indication of the locus for NS experiments along the vertical axis. Hyperfine experiments span all values of q, and depending on the temperature (κ) exhibit spin-nonconserving or Heisenberg behavior.

crossover temperature at zero wave vector.[44] This permits direct comparison of t_d as calculated in Eq. (40) and $t_x(\bar{q})$ as observed in experiments. For Fe and Ni $t_d \approx 3\times 10^{-4}$ and $t_x(\bar{q})/t_d \approx 30$. Hence, true dipolar interactions are too weak to explain the hyperfine experiments.

At the same time, the failure to observe crossover in neutron experiments is consistent with the hyperfine results. To illustrate, consider that for Ni, neutron scattering yields the empirical relation $\kappa = 2t^{0.7}$ Å^{-1}, which leads to predicted crossover radii of $q_d = \kappa_d = 0.007$ Å^{-1} and $q_x = \kappa_x = 0.08$ Å^{-1}. As shown in Fig. 13, the neutron data at T_c overlap q_d not at all, and q_x only to a minor extent. The situation for Fe is similar.

This leaves the question whether pseudodipolar interactions can explain the observed crossover. Since $t_x(\bar{q})$ must be somewhat less than $t_x(0)$, the result $t_x(\bar{q})/t_d \approx 30$ is reasonably consistent with the estimate $t_x(0)/t_d \approx 100$ based on Joenk's calculations of pseudodipolar strength. Pseudodipolar forces can therefore explain the data semiquantitatively; whether they constitute a unique explanation is not clear. As already noted, the observed T_c independence of $t_x(\bar{q})$ is also expected for spin-lattice forces.

3. *fcc Co*

In this case neutron experiments show no crossover as in the case of Fe and Ni, and hyperfine experiments of sufficiently asymptotic character have not been done. If the analysis of Fe and Ni is correct, crossover in fcc Co should occur at $t_x(\bar{q}) \approx 10^{-2}$.

4. *Cubic Fe_3O_4*

Here neutron experiments extend to $q = 0.03$ Å^{-1} and suggest incipient crossover to $z = 2$. Since cubic Fe_3O_4 exhibits macroscopic anisotropy comparable to that of Fe,[42] it is plausible that pseudodipolar forces are at work here as well. Hyperfine experiments to demonstrate crossover have not been done.

X. SUMMARY AND CONCLUSION

Our review of crossover phenomena in critical dynamics in isotropic ferromagnets leads to a plausible and consistent picture within the framework of dynamical scaling theory, with principal attributes that may be summarized as follows.

For the low-T_c S-state insulating systems EuS and EuO, no clearcut Heisenberg region has yet been identified. Instead, ESR experiments indicate a direct transition at $t = 10^{-2}$ from a noncritical region to a critical region with $z = 2$; and neutron experiments, insofar as they are available, indicate an "intermediate" exponent z between 2 and $\frac{5}{2}$. The most probable cause of this behavior is true dipolar interactions between freely orientable electronic spins, for which crossover temperature and wave vector are estimated to be $t_d = 5\times 10^{-2}$ and $q_d = 0.16$ Å^{-1}, in agreement with experiment.

For the high-T_c, non-S-state metallic systems Fe and Ni, hyperfine interaction experiments exhibit two critical regions. Far from $q = 0$, Heisenberg behavior with $z = \frac{5}{2}$ is seen. Near $q_x = 0.08$ Å^{-1} crossover to $z = 2$ occurs. Whereas dipolar interactions may be ruled out, pseudodipolar interactions discussed originally by van Vleck can explain the observed crossover temperature. The observed crossover in hyperfine experiments is consistent with the observation of pure Heisenberg behavior in neutron experiments because these lie largely in the range $q \geq 0.08$ Å^{-1}. If this analysis is correct, fcc Co and cubic Fe_3O_4 should exhibit behavior similar to that of Fe and Ni.

As plausible as this picture appears, there are some important questions which remain.

(1) Is the observation of crossover in Fe and Ni due to the use of hyperfine techniques, or would it show up in extended neutron experiments as well?

(2) Is there really no Heisenberg region in EuO and EuS, as suggested by ESR experiments, or would it appear in hyperfine experiments and extended neutron experiments?

(3) Can the observation of crossover in Ni and Fe be extended to other non-S-state systems, such as fcc Co and cubic Fe_3O_4, as would be suggested by the hypothesized effect of pseudodipolar interactions, or is crossover in fact due to other causes?

It seems clear that answers to these questions will provide interesting experimental tests of our understanding. If they have outcomes as expected, they would go a long way toward removing remaining puzzles about dynamical critical behavior of isotropic ferromagnets.

Beyond experiments it is, of course, important to probe further into the theoretical question: What detailed behavior is expected for each of several spin-nonconserving interactions? Theoretical work on the pseudodipolar and the spin-lattice interaction as perturbations of critical dynamics would be particularly desirable.

ACKNOWLEDGMENTS

This research was supported in part by the National Science Foundation under Grant No. DMR 80 02443 to Clark University. The work benefited from critical reading and checks of nuclear relaxation calculations by Gary S. Collins, W. W. Warren, and A. R. Chowdhury, discussions on critical dynamics theory with G. Mazenko, S. Ma, and H. Gould, and experimental assistance by Carl Allard, T. A. Kachnowski, and M. A. Kobeissi. In addition the work was stimulated by the ESR studies of A. M. Gottlieb and R. A. Dunlap, as noted in Sec. III. Irradiations of Rh targets were performed by A. Kohler at the Harvard Cyclotron.

---

*Present address: Department of Physics, University of North Carolina, Chapel Hill, North Carolina 27514.

†Present address: Department of Physics, Carnegie Mellon University, Pittsburgh, Pennsylvania 15213.

[1]R. M. Suter and C. Hohenemser, J. Appl. Phys. 50, 1814 (1979).

[2]P. C. Hohenberg and B. I. Halperin, Rev. Mod. Phys. 49, 435 (1977).

[3]R. M. Suter and C. Hohenemser, Phys. Rev. Lett. 41, 705 (1978).

[4]L. Chow, R. M. Suter, and C. Hohenemser, Phys. Rev. Lett. 45, 908 (1980).

[5]M. Shaham, J. Barak, U. El-Hanany, and W. W. Warren, Jr., Phys. Rev. B 22, 5400 (1980); Solid State Commun. 29, 835 (1979); Phys. Rev. Lett. 39, 570 (1977).

[6]B. I. Halperin and P. C. Hohenberg, Phys. Rev. 177, 952 (1969).

[7]J. Als-Nielsen, in *Phase Transitions and Critical Phenomena,* edited by C. Domb and M. S. Green (Academic, New York, 1976), Vol. 5a.

[8]H. E. Stanley, *Introduction to Phase Transitions and Critical Phenomena* (Oxford University Press, New York, 1971).

[9]H. E. Stanley, T. S. Chang, F. Harbus, and L. L. Liu, in *Local Properties at Phase Transitions,* edited by K. A. Müller and A. Rigamonti (North-Holland, Amsterdam, 1976).

[10]V. J. Minkiewicz, M. F. Collins, R. Nathans, and G. Shirane, Phys. Rev. 182, 624 (1969).

[11]M. F. Collins, V. J. Minkiewicz, R. Nathans, L. Passell, and G. Shirane, Phys. Rev. 179, 417 (1969). See also V. J. Minkiewicz, Int. J. Magn. 1, 149 (1971).

[12]C. J. Glinka, V. J. Minkiewicz, and L. Passell, Phys. Rev. B 16, 4084 (1977).

[13]O. W. Dietrich, J. Als-Nielsen, and L. Passell, Phys. Rev. B 14, 4923 (1976).

[14]O. Steinsvoll, F. Mustoe, L. M. Corliss, and J. M. Hastings, Phys. Rev. B 14, 4190 (1976).

[15]R. A. Dunlap and A. M. Gottlieb, Phys. Rev. B 22, 3422 (1980).

[16]J. Kötzler, W. Scheithe, R. Blickhan, and E. Kaldis, Solid State Commun. 26, 641 (1978).

[17]J. Kötzler, G. Kamleiter, and G. Weber, J. Phys. C 9, L361 (1976).

[18]J. Kötzler and W. Scheithe, J. Magn. Magn. Mater. 9, 4 (1978); see also J. Kötzler and H. von Philipsborn, Phys. Rev. Lett. 40, 790 (1978).

[19]A. Abragam, *The Principles of Nuclear Magnetism* (Oxford University Press, London, 1962).

[20]A. Abragam and R. V. Pound, Phys. Rev. 92, 943 (1953).

[21]H. Gabriel, Phys. Rev. 181, 506 (1969).

[22]E. Bradford and W. Marshall, Proc. Phys. Soc. London 87, 731 (1966).

[23]R. C. Reno and C. Hohenemser, in *Proceedings of the Seventeenth Annual Conference on Magnetism and Magnetic Materials,* edited by D. C. Graham and J. J. Rhyne (AIP, New York, 1972).

[24]A. M. Gottlieb and C. Hohenemser, Phys. Rev. Lett. 31, 1222 (1973).

[25]M. A. Kobeissi, R. M. Suter, A. M. Gottlieb, and C. Hohenemser, Phys. Rev. B 11, 2455 (1975).

[26]M. A. Kobeissi and C. Hohenemser, Hyperfine Interact. 41, 705 (1978). See also M. A. Kobeissi, Phys. Rev. B 24, 2380 (1981).

[27]T. Kachnowski, R. M. Suter, A. M. Gottlieb, and C. Hohenemser, Phys. Rev. B 14, 5022 (1976).

[28]J. S. Evans, Ph.D. dissertation, Princeton University, 1965 (unpublished).

[29]M. A. Kobeissi and C. Hohenemser, Rev. Sci. Instrum. 49, 601 (1978).

[30]M. J. L. Yates, in *Alpha, Beta and Gamma-ray Spectroscopy,* edited by K. Siegbahn (North-Holland, Amsterdam, 1966).

[31]R. C. Reno, Ph.D. dissertation, Brandeis University, 1970 (unpublished).

[32]A. R. Arend, C. Hohenemser, F. Pleiter, H. deWaard, L. Chow, and R. M. Suter, Hyperfine Interact. 8, 191 (1980).
[33]J. C. LeGuillou and J. Zinn-Justin, Phys. Rev. Lett. 39, 95 (1977).
[34]R. C. Reno and C. Hohenemser, Phys. Rev. Lett. 25, 1007 (1970).
[35]R. D. Lowde, J. Appl. Phys. 36, 884 (1965).
[36]J. A. Hertz, J. Magn. Magn. Mater. 1, 253 (1971); 1, 307 (1971); 1, 303 (1971).
[37]D. L. Huber, J. Phys. Chem. Solids 32, 2145 (1971).
[38]S. V. Maleev, Zh. Eksp. Teor. Fiz. 66, 1809 (1974) [Sov. Phys.—JETP 39, 889 (1974)].
[39]G. B. Teitelbaum, Pis'ma Zh. Eksp. Teor. Fiz. 21, 339 (1975) [JETP Lett. 21, 154 (1975)].
[40]R. Raghavan and D. L. Huber, Phys. Rev. B 14, 1185 (1976).
[41]J. H. van Vleck, Phys. Rev. 52, 1137 (1937).
[42]R. M. Bozorth, *Ferromagnetism* (Van Nostrand, Princeton, 1951), Chap. 12.
[43]R. J. Joenk, Phys. Rev. 130, 932 (1963).
[44]To see why $t_x(\vec{q}) < t_x(0)$, consider a hyperfine measurement at some value $t < t_x(0)$. Then the integral for τ_c given in Eq. (20) will run along a line defined by $\kappa = \kappa_0 t^{\nu}$, a vertical line in Fig. 12. For $q > q_x$, this line will be in the Heisenberg region. Crossover to Heisenberg behavior will occur in τ_c when t is close enough to $t_x(0)$ so that an appreciable fraction of the integrand lies in the Heisenberg region.